Accounting for El Niño-Southern Oscillation influence becomes urgent for predicting future East African ecosystem responses

Istem Fer [1,2,3], Britta Tietjen [4,5], Florian Jeltsch [1,5], Christian Wolff [6,7]

[1] Department of Plant Ecology and Nature Conservation, Institute of Biochemistry and Biology, University of Potsdam, Am Mühlenberg 3, 14476 Potsdam, Germany.

[2] DFG Graduate School Shaping the Earth's Surface in a Variable Environment, University of Potsdam, Karl-Liebknecht-Str. 24, 14476 Potsdam, Germany.

[3] Department of Earth and Environment, Boston University, 675 Commonwealth Avenue, 02215 MA, USA.

[4] Biodiversity and Ecological Modelling, Institute of Biology, Freie Universität Berlin, Altensteinstr. 6, 14195 Berlin, Germany.

[5] Berlin-Brandenburg, Institute of Advanced Biodiversity Research (BBIB), D-14195 Berlin, Germany.

[6] Climate Geochemistry Department, Max-Planck Institute for Chemistry, Hahn-Meitner Weg 1, 55128 Mainz, Germany.

[7] International Pacific Research Center, School of Ocean and Earth Science and Technology, University of Hawai'i at Manoa, Honolulu, 96822 HI, USA.

Correspondence to: Istem Fer (fer.istem@gmail.com)

Abstract. The El Niño Southern Oscillation (ENSO), is the main driver for the interannual variability in East African rainfall with significant impact on vegetation and agriculture, and dire consequences for food and social security. In this study, we identify and quantify the ENSO contribution to the East African rainfall variability to forecast future East African vegetation response to rainfall variability related to a predicted intensified ENSO. To differentiate the vegetation variability due to ENSO, we removed the ENSO signal from the climate data using Empirical Orthogonal Teleconnections (EOT)

analysis. Then, we simulated the vegetation under the historical climate without components related to

ENSO teleconnections. We found ENSO driven patterns in vegetation response and confirmed that EOT

25   analysis can successfully produce coupled tropical Pacific Sea Surface temperature-East African rainfall

teleconnection from observed datasets. We further simulated East African vegetation response under

future climate change as it is projected by climate models and under future climate change combined

with a predicted increased ENSO intensity. Our EOT analysis highlight that climate simulations are still

not good at capturing rainfall variability due to ENSO, and as we show here the future vegetation would

30   be different from what is simulated under these climate model outputs lacking accurate ENSO

contribution. We simulated considerable differences in East African vegetation growth under the

influence of an intensified ENSO regime which will bring further environmental stress to a region with

a reduced capacity to adapt effects of global climate change and food security.

1 Introduction

35   The 2010-2011 drought in the Horn of Africa, by some measures the worst drought in 60 years

(Nicholson, 2014), is a reminder that rainfall in this politically and socioeconomically vulnerable region

can fluctuate dramatically. El Niño Southern Oscillation (ENSO) influence has long been at the center

of attention as a driver of this interannual fluctuations in East African rainfall (Indeje et al. 2000, Anyah

and Semazzi, 2007, Nicholson, 2015), however, it is still an on-going endeavour to qualify and quantify

40   the future behaviour of ENSO regimes under the predicted future warming (Vecchi & Wittenberg, 2010;

Miralles et al., 2014). In this study we aim to identify and quantify the ENSO contribution to the East

African rainfall variability in order to increase our understanding on the future response of East African

vegetation to rainfall variability related to changing ENSO regimes and climate which can have dire consequences in this region in terms of food and social security.

1.1 East African climate

Rainfall in East African climate is primarily controlled by the seasonal passage of the Intertropical Convergence Zone (ITCZ) (Nicholson, 2000). While mean annual precipitation varies from <200 to >2000mm/year (Nicholson, 2000) and dry season length can vary from 0 to >8 months. Interannual variations in the seasonal migration of the East African ITCZ are driven to large extent by the ENSO (Ropelewski and Halpert, 1996) and its related impact through western Indian Ocean sea surface temperature (SST) anomalies (Goddard and Graham, 1999). The effect of ENSO on East African precipitation is diversified. Surface ocean warming in the western Indian Ocean (El Niño) leads to intensification and shifts of the ITCZ, bringing more precipitation to East Africa (Wolff et al., 2011), even through the direct teleconnection through the atmosphere tends to reduce rainfall (La Niña). These regions receive above average rainfall in El Niño years and below average in La Niña years during the OND months (Endris et al., 2013).

1.2 East African vegetation

The control ENSO exerts on East African precipitation also manifests itself on the vegetation which is contingent upon the seasonal rainfall. East Africa hosts a variety of biomes ranging from tropical rainforest to desert, however the region is mainly dominated by arid or semi-arid vegetation (Bobe, 2006). The arid and semi-arid vegetation consist of species that can tolerate aridity for several months

as a result of the exceedingly seasonal precipitation (Bobe, 2006). Agricultural activities also depends on this strong seasonality as it determines the cropping times (Shisanya et al., 2011). Maize, beans, coffee, tea and wheat are among the important agricultural products of East Africa together with fruit products, and grasses for livestock (FAOSTAT, 2016).

An adaptive management of the limited resources will shape the future severity of climate change impacts on food productivity in this rainfall-reliant setup (Thornton et al., 2014). Therefore, a temporally and spatially extensive understanding of how the ecosystem dynamics in the region will respond to changing climate, and of particular concern to East Africa, to the ENSO regimes is needed. Several studies related the variability in African vegetation to ENSO events (Shisanya et al, 2011; Ivory et al., 2013; Abdi et al., 2016; Detsch et al., 2016). However, the forthcoming of this relationship has been less of a focus, partly due to our imperfect knowledge on the nature of the future ENSO response to changing climate.

1.3 ENSO impact on East African vegetation

An opportunity to examine the ENSO – East African vegetation relationship is by means of using predictive tools such as vegetation models which have been successfully applied to determine and forecast regional vegetation dynamics (Moncrieff et al., 2014; Scheiter and Savadogo, 2016) as well as agricultural yields (Waha et al., 2013; Dietrich et al., 2014). In this study, we used the latest climate projections from the Intergovernmental Panel on Climate Change (IPCC) 5th assessment report for Representative Concentration Pathway (RCP) 8.5 scenario, downscaled by the Coordinated

Downscaling Experiment (CORDEX) (Nikulin et al., 2012, Endris et al., 2013) to drive such a process-based dynamic vegetation model, LPJ-GUESS (Lund-Potsdam-Jena general Ecosystem Simulator). To be able to differentiate the vegetation variability due to ENSO, we removed the ENSO signal from the climate data and simulated the vegetation under the historical climate without components related to

85   ENSO teleconnections. Here we aim to look at the ENSO influence on East African vegetation i) under present conditions, ii) under projected future climate, and iii) under a potentially increased ENSO intensity combined with future climate change. Finally, we discuss the effects of ENSO-related vegetation variability on the carbon and hydrological cycles, and its significance for mitigation efforts in the region.

90

2 Methods

2.1 The LPJ-GUESS model

We used the dynamic vegetation model LPJ-GUESS (Lund-Potsdam Jena General Ecosystem Simulator, Smith et al. 2001; Sitch et al. 2003, Gerten et al. 2004), for our study. LPJ-GUESS is a

95   mechanistic model in which ecosystem processes are simulated via explicit equations and is optimised for regional to global applications (Smith et al., 2001; Sitch et al., 2003; Gerten et al., 2004). Vegetation dynamics are simulated as the emergent outcome of growth, reproduction, mortality and competition for resources among woody plant individuals and herbaceous vegetation.

The simulation units in this study are plant functional types (PFTs) distinguished by their growth form,

100   phenology, photosynthetic pathway (C_3 or C_4), bioclimatic limits for establishment and survival and, for

woody PFTs, allometry and life history strategy. The simulations of this study were carried out in

'cohort mode,' in which, for woody PFTs, cohorts of individuals recruited in the same patch in a given

year are represented by a single average individual, and are thus assumed to retain the same size and

form as they grow. A sample instruction file used to run LPJ-GUESS in this study with all the

105   parameters listed can be found under github.com/istfer/ENSOpaper/ins.

Primary production and plant growth follow the approach of LPJ-DGVM (Sitch et al. 2003). Population

dynamics (recruitment and mortality) are influenced by available resources and environmental

conditions, and depends on demography and the life history characteristics of each PFT (Hickler et al.

2004). Disturbances such as wildfires are simulated based on temperature, fuel load and moisture

110   availability (Thonicke et al. 2001). Litter arising from phenological turnover, mortality and disturbances

enters the soil decomposition cycle. Decomposition rates depend on soil temperature and moisture

(Sitch et al. 2003). Soil hydrology follows Gerten et al. (2004). A more detailed description of LPJ-

GUESS is available in Smith et al. (2001). We used LPJ-GUESS version 2.1 which includes the PFT set

and modifications described in Ahlström et al. (2012). LPJ-GUESS has already been successfully

115   applied and validated to match present-day observed biome distributions of East Africa (Fer et al.,

2016).

2.2 Datasets Tracking ENSO and regional vegetation

2.2.1 ENSO

120   To isolate the ENSO signal contribution to East African precipitation, we conducted an Empirical

Orthogonal Teleconnections (EOT) analysis between sea surface temperatures (SSTs) in the tropical

pacific ocean and precipitation over East Africa (see section *Identifying the ENSO signal*). For historical

extraction (1951-2005), we use monthly National Oceanic and Atmospheric Administration Extended

Reconstructed Sea Surface Temperature (NOAA ERSST) V4 dataset (Huang et al., 2014; Liu et al.,

125   2014), available on 2ºx2º global grids as a predictor field. As the response series, we used monthly

Climatic Research Unit Time Series (CRU TS) 3.20 dataset (Harris et al., 2014), available on 0.5ºx0.5º

global grids.

2.2.2 LPJ-GUESS datasets

LPJ-GUESS requires monthly climate (temperature, precipitation, cloud cover), atmospheric CO_2

130   concentration and soil texture as input data. For historical period (1951-2005), we used monthly CRU

TS 3.20 climate data. We chose these years for all historical analysis throughout the study as the

historical simulations of CORDEX outputs are available for this period. For future projections (2006-

2100), we used the outputs from the Coordinated Regional Climate Downscaling Experiment

(CORDEX) program for the Africa domain. For the future scenario, we chose high emissions

135   Representative Concentration Pathways (RCP) 8.5 scenario as this is considered as the baseline scenario

under the assumption that climate mitigation targets will not be met (Moss et al., 2010; Riahi et al.,

2011). This is a reasonable choice given that the observed trends are pointing beyond RCP 8.5 trajectory (Sanford et al., 2014). CORDEX, downscaled global climate models (GCMs) by using regional models, and the outputs are available from ESGF-CoG data portal (https://pcmdi.llnl.gov/search/esgf-llnl/). For

140   East African climate, we took the ensemble mean of 9 downscaled models for future projections of RCP 8.5 scenario: CCCma CanESM2, CERFACS CNRM-CM5, QCCCE CSIRO Mk3-6-0, ICHEC EC-EARTH, IPSL CM5A-MR, MIROC5, MPI ESM-LR, NCC NorESM1-M, NOAA GFDL-ESM2M (Full names of the models are given in the Appendix). Instead of working with individual models we decided to drive our simulations with ensemble means as it has been shown to outperform individual models and

145   show a better agreement with data (Endris et al., 2013). RCP 8.5 compatible atmospheric CO_2 values were also used as provided by NOAA – GISS experiment (Nazarenko et al., 2015).

2.2.3 Bias correction

To eliminate biases originating from using CRU climate dataset for present and model simulations for future, we subtract the 1951-2005 climatology of downscaled GCM ensemble from the 1951-2100 time

150   series of the ensemble and add the anomalies on CRU 1951-2005 climatology. This way we will able to have a meaningful comparison between CRU-driven and GCM-driven vegetation model outputs while keeping the climate variability from the GCM simulations. We should note here, that this would not change the ENSO signal we will retrieve from the GCM outputs (see next section) because we de-season and work with anomalies of the data field for our EOT analysis.

155

2.2.4 Future Pacific SSTs

For future pacific SSTs, we used outputs from GCM simulations of the same models listed above for RCP 8.5, except ICHEC EC-EARTH which was not available from the data portal at the time. However, these GCM outputs were not downscaled and standardized in terms of spatial resolution (they were all available in monthly time steps in terms of temporal resolution). We created raster files from these outputs and using the "raster-package" (R Core Team, 2015; v2.5-8), we resampled these rasters to brought them to the same spatial resolution as NOAA ERSST V4 dataset, and we took the ensemble mean.

2.3 Identifying the ENSO signal

Here we first identify the ENSO signal as a driver for monthly East African precipitation variability over the historical period (1951-2005). To do this we investigate the teleconnectivity between the SSTs in the tropical Pacific Ocean and precipitation over East Africa by using empirical orthogonal teleconnections (EOT). The method is explained by van den Dool et al. (2000) in detail, and Appelhans et al. (2015) implemented the original algorithm in R ('remote' package by Appelhans et al., 2015; R Core Team, 2015). Here, we only briefly present the major steps of the EOT analysis:

2.3.1 Empirical Orthogonal Teleconnections (EOT)

In the EOT analysis, we aim to establish an explanatory relationship between the temporal dynamics of a (predictor) domain and temporal variability of another (response) domain. Such predictor and response domains consist of gridded time series profiles: in this study the gridded monthly SST time

175   series of the tropical pacific as predictor and gridded precipitation time series of East Africa as the

response. Then, the first step of EOT analysis is to regress these time series of each predictor domain

grid (N_p) against the time series of each response domain grid (N_r) (Appelhans et al., 2015). This will

result in a (N_p x N_r) number of regression fits after which we can calculate the sum of coefficients of

determination per predictor grid (ending up with N_p sum of coefficients of determination values). Then,

180   the grid with the highest sum will be identified as the "base point" of the leading mode as it explains the

highest portion of the variance in the response domain (Appelhans et al., 2015). The time-series at this

base point is referred as the leading teleconnection, or hereafter as the first EOT.

2.3.2 Screening for ENSO signal

We applied the EOT method on de-seasoned and de-noised data fields in order to retrieve a low

185   frequency signal such as ENSO: here we used the SSTs in the tropical pacific ocean as predictor and

precipitation over East Africa as response. Then we proceeded to calculate the SSTs modes that are most

affecting for East African rainfall variability. We found the 1st EOT to be the ENSO signal. We

compared this EOT with Nino3.4 index to see whether we were able to isolate the ENSO signal. The

commented code used for all methods is publicly available on Github (github.com/istfer/ENSOpaper).

190   Before moving on to identifying future pacific sea surface temperature – East African precipitation

interactions, we applied the same extraction to historical GCM outputs (simulations) to see whether we

can identify a similar relationship from GCM products. Finally, we prepared the model drivers with the

modified ENSO signal we identified from the future simulations (see next section) and ran the model

with these datasets (here we focused on precipitation data only, while precipitation varies in these

195   simulations and the others -temperature- were kept as they were in the climate datasets: present – CRU

TS 3.2, future – CORDEX ensemble de-biased using CRU as explained above).

2.4 Removing and intensifying the ENSO signal

In order to investigate the contribution of the ENSO signal to East African precipitation, we removed

200   the ENSO signal and explored the rainfall pattern with and without ENSO contribution as well as the

resulting vegetation changes calculated by LPJ-GUESS. We used the "remote" package which

specifically implements the EOT analysis and keeps track of calculated values in a structured workflow:

The rainfall we are left with after removing the first EOT mode (which we identified as the ENSO

signal) becomes the rainfall behaviour without ENSO contribution (within the 'remote' package, this

205   calculation of the residuals is automatically available after the calculation of the EOT modes).

Therefore, if we take the difference between these residuals and the initial de-seasoned and de-noised

data, this will give us the amount that we need to subtract from the raw data field to obtain the rainfall

behaviour without ENSO contribution. The steps are explained below as pseudocode:

i) Deseason and denoise the response and predictor fields.

210    $EA_{r, ds, dns}$: East African precipitation (response domain). Subscripts indicate raw, deseasoned, deseasoned

and denoised respectively.

$PAC_{r, ds, dns}$: Tropical Pacific Ocean Sea Surface Temperatures (SSTs) (predictor domain). Subscripts

indicate raw, deseasoned, deseasoned and denoised respectively.

$$EA_{ds} = deseason(EA_r) \qquad PAC_{ds} = deseason(PAC_r) \qquad (1)$$

215 $\qquad EA_{dns} = denoise(EA_{ds}) \qquad PAC_{dns} = denoise(PAC_{ds}) \qquad (2)$

ii) Conduct Empirical Orthogonal Teleconnection (EOT) analysis:

$$EOT_{modes} \leftarrow EOT(EA_{dns} \sim PAC_{dns}) \qquad (3)$$

Here the EOT_{modes} object can be thought as a list that stores both the time series of the modes, the

reduced fields obtained after the removal of each mode, slopes and intercepts of the fields (for more

220 details see Appelhans et al., 2015).

iii) Calculate the difference (*Diff*) between the de-seasoned, de-noised data (EA_{dns}) and the rainfall

behaviour without ENSO contribution from the information that is already stored in the resulting

EOT_{modes} object (ENSO signal is the first mode, therefore the rainfall behaviour we are left without

ENSO will be the $EA_{modes, rr1}$ where subscript *rr1* indicating "response residual" after the removal of the

225 first EOT mode:

$$Diff = EA_{dns} - EA_{modes, rr1} \qquad (4)$$

iv) If we subtract this difference from the initial raw response field (EA_r), we will obtain the East

African precipitation without ENSO contribution ($EA_{r, woENSO}$):

$$EA_{r, woENSO} = EA_r - Diff \qquad (5)$$

230 v) As EOT analysis is basically a regression analysis, we can also obtain the ENSO contribution (*Diff*)

from the regression equation as shown below (which will become handy when we insert back the

intensified ENSO signal):

$$Diff = EOT_{modes, eot\_1} * EOT_{modes, ri\_1} - EOT_{modes, rs\_1} \qquad (6)$$

Here EOT_{modes, eot_1}, EOT_{modes, ri_1} and EOT_{modes, rs_1} refer to the EOT time series of the 1st mode (the ENSO

235 signal), intercept of and slope of the response field calculated for the 1st mode (Appelhans et al., 2015).

vii) Then, it is possible to modify the future ENSO signal (EOT_{modes, eot_m}) obtained from EOT analysis on

simulation datasets, re-calculate its contribution to the East African rainfall ($Diff_{new}$) and add this amount

back on the precipitation data without ENSO signal ($EA_{r, woENSO}$) to obtain new precipitation amounts

($EA_{r, new}$) due to new signal. We can later use this $EA_{r, new}$ as the future precipitation input to our

240 vegetation model to drive future simulations.

$$Diff_{new} = EOT_{modes, eot\_m} * EOT_{modes, ri\_1} - EOT_{modes, rs\_1} \qquad (7)$$

$$EA_{r, new} = EA_{r, woENSO} + Diff_{new} \qquad (8)$$

Here it is noticable that slope(s) and intercept(s) would also have been different if the ENSO signal was

changes (EOT_{modes, eot_m}). However, this simplification is adequate for experiments in this paper.

245 Moreover, we used the intercept and slope we retrieved from the EOT analysis on observational datasets

while re-calculating the new difference ($Diff_{new}$) due to intensified ENSO signal. Because the East

African rainfall patterns explained by Tropical Pacific SSTs in the GCM simulations are different from observations (Figure A1 and A2). By using slopes and intercepts obtained from the observational data we were also able to preserve the more accurate patterns in rainfall differences.

250   viii) Finally, we obtained the modified ENSO signal (EOT_{modes, eot_m}) in Eq. (7) by detrending (fitting a LOWESS smoother and removing it from the signal) and multiplying the ENSO signal we extracted from the future simulations (deseasoned and denoised GCM simulations for East African rainfall – EA_{dns_ftr} - and Tropical Pacific SSTs - PAC_{dns_ftr} -) with a coefficient (k = 3) such that the peaks of the new signal would be as strong as the observed anomalies ($\pm$ 2.5 °C, Figure 1 and S3). For the code of

255   this step see IdentifyModifyFutureENSO.R script at github.com/istfer/ENSOpaper.

$$EOT_{modes\_ftr} \leftarrow EOT(EA_{dns\_ftr} \sim PAC_{dns, ftr}) \tag{9}$$

$$EOT_{modes, eot\_m} \leftarrow k * detrend(EOT_{modes\_ftr, eot\_1}) \tag{10}$$

3 Results

260   **3.1 EOT analysis- extracting the ENSO signal**

We compared the first EOT mode extracted after de-seasoning and de-noising the fields as explained by Appelhans et al. (2015) to the Nino-3.4 index recorded (Figure 1). The high correlation between the two (R = 0.90) confirms that we were able to extract the ENSO signal by conducting the EOT analysis. On the predictor domain (Tropical Pacific SSTs), the Nino-3.4 region found to be the area which explains

265   the most variance in the response domain (East African precipitation) as expected (Figure A1). The time

series of the first EOT explains 0.85% of the rainfall variability over the analyzed period here (1951-

2005). This small amount is not surprising, because East African precipitation follows a strong seasonal

pattern following the position of the Intertropical Convergence Zone (ITCZ) within the year. Therefore,

seasonality alone explains most of the variability in East African rainfall. In addition, due to the

270   complex topographical setting of the region, local conditions play a major role in the variation of the

rainfall. Still, when we de-season and de-noise the raw data fields to identify low-frequency signals

such as ENSO, the ENSO signal emerged as the most important teleconnection between tropical pacific

SST anomalies and East African precipitation.

Having successfully extracted the ENSO signal from the observation datasets, we applied the same

275   procedure with the outputs of the climate models. We used an ensemble of SSTs from 8 GCM outputs as

the predictor field and an ensemble of rainfall from 9 GCMs downscaled by CORDEX as the response

domain. The comparison between the calculated first EOT time series to the Nino-3.4 index observed

was much poorer (R=0.19) (Figure 1) which indicates that GCMs are not capturing the coupled Pacific

SST – East African rainfall teleconnection. Another striking feature that can be observed in Figure 1 is

280   the smoothness of the time series of the 1st mode calculated from the EOT analysis on ensembles of

climate model outputs when compared to the recorded index and the calculated ENSO signal from the

observation datasets. In other words, the ENSO signal retrieved from the EOT analysis on the climate

model outputs is nowhere near strong as the others. According to this signal obtained from the

simulation datasets, the only ENSO events that happened during 1951-2005 period were in the "weak"

285   category (Figure 1). Finally, the calculated patterns were different than the EOT analysis on observed

        datasets (the corresponding figure is given in the Appenix, Figure A2): The areas where the sum of the

        coefficients of determination were the highest were again situated around Nino 3.4 region but closer to

        the Nino 4 region this time (Figure A2 – left panel). Spatially, the north-eastern and central parts of the

        response domain are the most explained whereas previously it was more centralized around the coastal

290   equatorial parts of the region (Figure A2 – right panel).
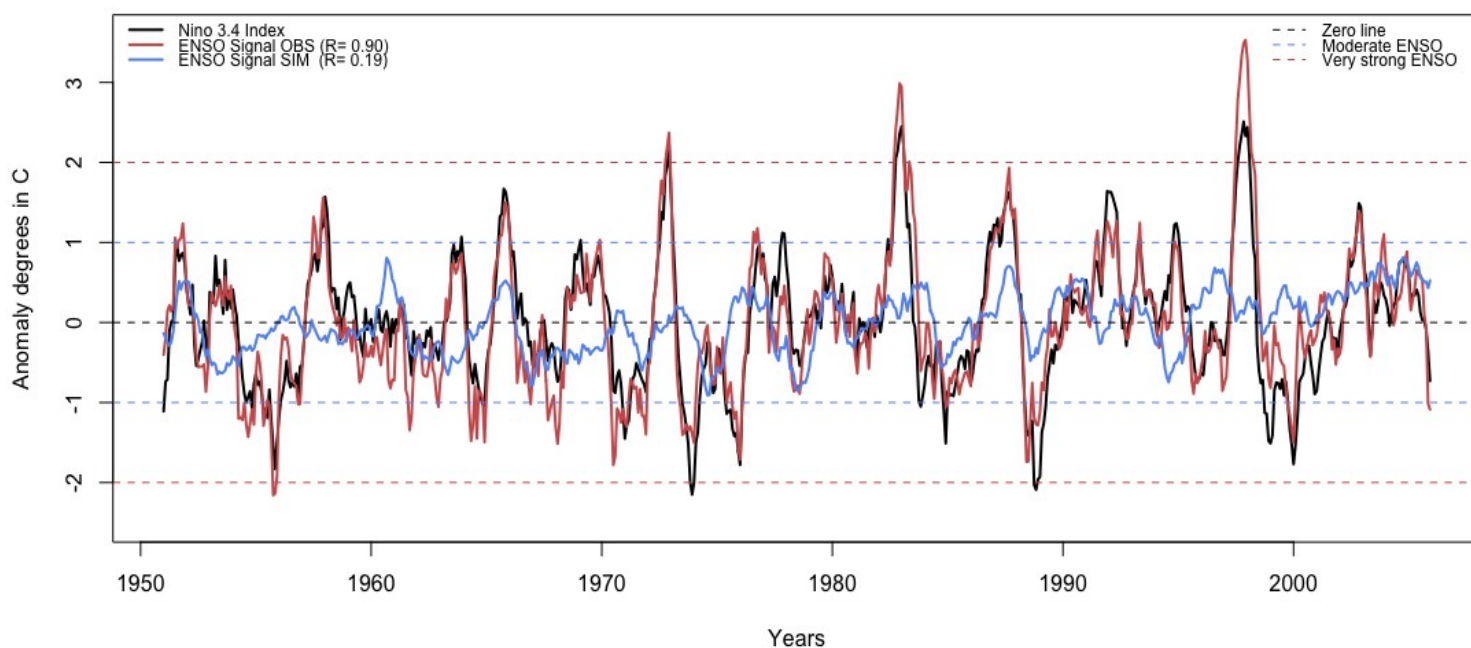
Figure 1. The comparison between Nino 3.4 Index recorded by NOAA (black line), time series of the 1st mode

obtained from the EOT analysis on observed CRU-NOAA datasets (red), and time series of the 1st mode obtained

from the EOT analysis on ensembles of the climate model simulations (blue). Black dashed line: Zero line. Blue

dashed lines ± 1.0° anomaly thresholds for categorizing moderate ENSO events. Red dashed lines: ±

295   2.0° anomaly thresholds for categorizing very strong ENSO events.

3. 2 Historical simulations with and without the ENSO signal

After calculating the ENSO signal, we removed the amount due to ENSO from the East African precipitation (CRU precipitation), and simulated East African vegetation using both datasets (CRU$_{normal}$

300 and CRU$_{without\_ENSO}$) to see its effect on vegetation. As it can clearly be seen from Figure 1, impact of ENSO signal is not the same everywhere on the East African domain, which means removing ENSO signal would have differential effects on the rainfall amount. Regional maps of rainfall anomalies for the strongest three El Niño (1972, 1982, 1999) and La Niña (1973, 1975, 1988) events between 1951-2005 period are given in Figure 2. Here we show what the rainfall would be if there were not any

305 influence by the Pacific SSTs particularly during these three years. Especially the coastal Kenya and Tanzania experience a strong change in the amount of rainfall they receive: During the El Niño periods, these parts of East Africa receive up to 200 mm yr^{-1} more rain other than they would receive, while they receive ~100 mm yr^{-1} less rain during the La Niña years. The impact is the opposite for western part of Ethiopia : receiving ~200 mm yr^{-1} less rainfall during El Niño years, while ~100 mm yr^{-1} more during

310 La Niña years. To provide a closer look to the impacts of ENSO related variability on vegetation, we report the results on vegetation simulations within the two transects where we see the strongest impacts over these two oppositely behaving, coastal and northwestern, regions (Fig. 2).
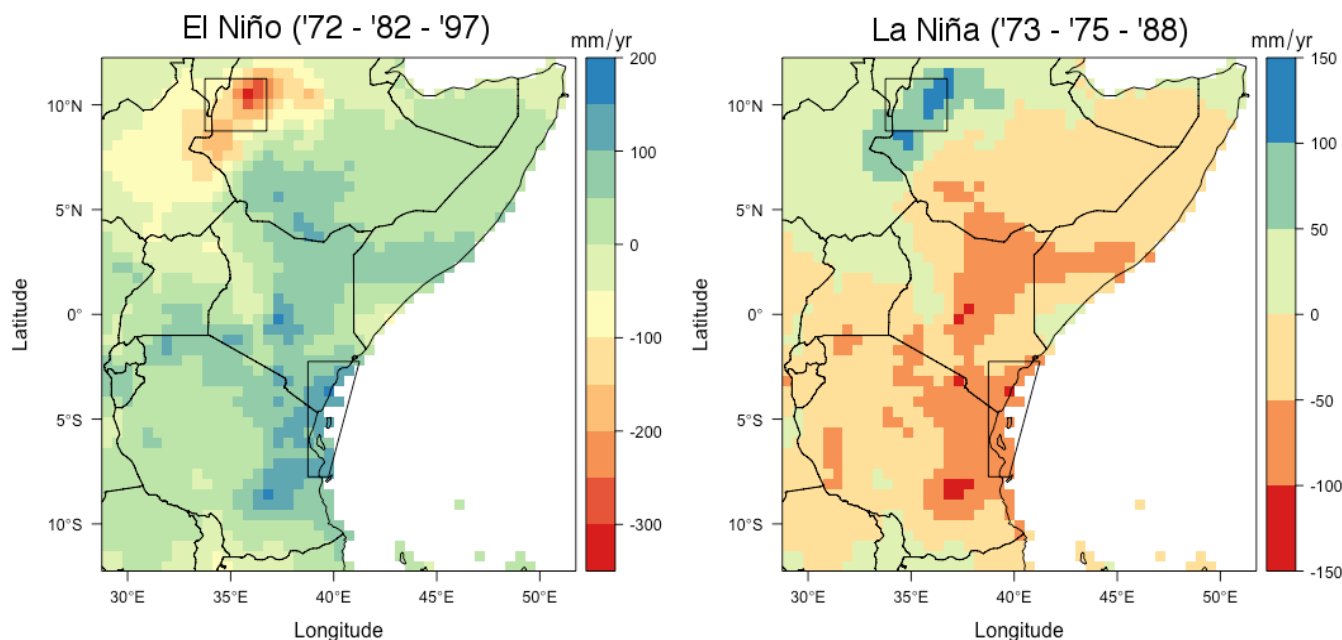
Figure 2. Regional maps of anomalies (mm yr^{-1}) for the strongest three (1972, 1982, 1997) El Niño (left) and (1973, 1975, 1988) La Niña (right) events between 1951-2005 period (anomalies were calculated by subtracting precipitation without ENSO contribution from precipitation with ENSO contribution). Northern inner and southern coastal transects chosen for reporting results on vegetation simulations.

We drove the dynamic vegetation model once with CRU dataset as is and once with CRU dataset with removed ENSO contribution. Results are reported for the previously mentioned north and south sites in Figure 3 and Table 1. Outputs from the northern-inner part show more variability within the chosen grid-cells for this region. Indeed, this region is on the western edge of Ethiopian Plateau, with a transition of biomes from mountainous forests to woodlands and savannas (Fer et al., 2016). As the rainfall patterns in relation to ENSO signal was the opposite between these regions (Figure 2), we expect to see that the response of these regions to the removal of the ENSO signal to be opposite, and

this is indeed what we see in Figure 3: While outputs such as net primary productivity (NPP), net ecosystem exchange (NEE), soil evapotranspiration (EVAP) and surface runoff (RUNOFF) for northern site were less than otherwise they would be for El Nino events, they would be higher La Nina events. And the opposite behaviour is true for the southern site.
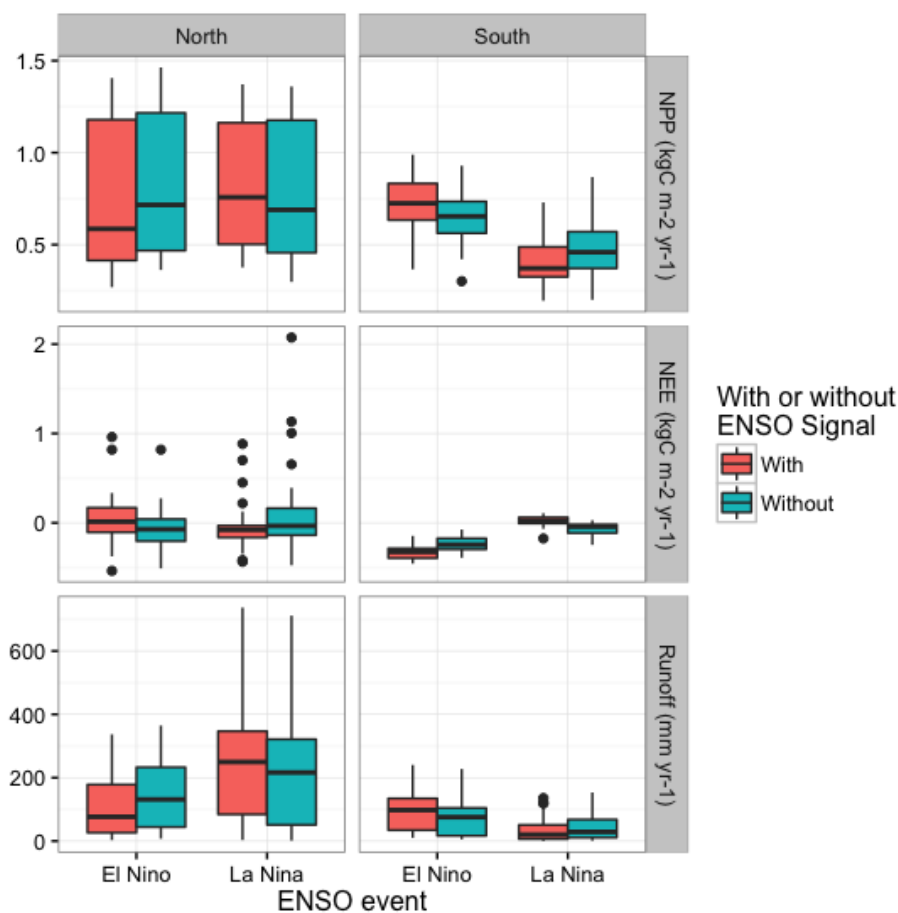
Figure 3. Carbon and water fluxes from north and south transects, simulated under climate with and without ENSO contribution, for the strongest three (1972, 1982, 1997) El Niño and (1973, 1975, 1988) La Niña events between 1951-2005 period. Top panel: Net Primary Productivity (NPP). Middle: Net Ecosystem Exchange (NEE). Bottom: Total runoff. Locations of the northern-inner and southern-coastal sites are given in Figure 2.

335 In order to test whether the difference between the vegetation simulated under climate with ENSO contribution, and the vegetation simulated under climate with removed ENSO contribution, we conducted a paired t-test on the outputs. The results (Table 1) show that except NEE for northern sites, all differences between the vegetation simulated with and without ENSO impact were significant. In summary, ENSO contribution is significantly affecting the East African vegetation and we would expect different vegetation if there were no ENSO events.

340

345

350

Table 1. Paired t-test results to test whether there is a significant difference in the vegetation simulations that are driven with and without ENSO contributions for the three strongest ENSO events during the historical period (1951-2005) and with and without intensified ENSO signal for the strongest ENSO events during the future period (2006-2100). Grey highlighted cells indicate insignificant differences according to p=0.05 threshold. Significant p-values indicate rejection of the H_0 in favor of the alternative, that is true difference in means is not equal to 0. p: p-value, md: mean of the differences

NPP: Net Primary Productivity, NEE: Net Ecosystem Exchange, RUNOFF: Surface runoff). Location of North (N) and South (S) sites are shown on Figure 2.

		NPP ($kgC\ m^{-2}\ yr^{-1}$)		NEE ($kgC\ m^{-2}\ yr^{-1}$)		RUNOFF ($mm\ yr^{-1}$)	
		El Niño	La Niña	El Niño	La Niña	El Niño	La Niña
Historical	N	$p < 0.05$ md: -0.056	$p < 0.05$ md: 0.035	$p = 0.089$	$p = 0.1$	$p < 0.05$ md: -41.35	$p < 0.05$ md: 22.21
Historical	S	$p < 0.05$ md: 0.084	$p < 0.05$ md: -0.074	$p < 0.05$ md: -0.088	$p < 0.05$ md: 0.087	$p < 0.05$ md: 19.41	$p < 0.05$ md: -10.74
Future	N	$p < 0.05$ md: -0.052	$p < 0.05$ md: 0.033	$p = 0.93$	$p = 0.58$	$p < 0.05$ md: -10.91	$p < 0.05$ md: 46.97
Future	S	$p < 0.05$ md: 0.049	$p < 0.05$ md: -0.101	$p < 0.05$ md: -0.113	$p < 0.05$ md: 0.173	$p < 0.05$ md: 5.66	$p = 0.06$

360   We conducted the same paired t-test for the north and south sites for the future simulations (Table 1). In the northern site where intensified signal leads to less (more) NPP during El Niño (La Niña) years, the mean difference is -52 (+32.6) gC m^{-2} yr^{-1} between the vegetation simulated under future climate with and without intensified ENSO signal. In the southern site where intensified signal leads to more (less) NPP during El Niño (La Niña) years, the mean difference is +49.1 (-101.1) gC m^{-2} yr^{-1} between the

365   vegetation simulated under future climate with and without intensified ENSO signal. While the mean differences for NEE were not significant at the northern site, southern site stores 112.7 (173.1) gC m^{-2} yr^{-1} more (less) carbon under the intensified ENSO scenario during the El Niño (La Niña) years.

Another noteworthy output is that, the northern site has a lot more runoff during the La Niña years under the intensified ENSO scenario. This is especially clear on Figure 4 where spatial patterns of the

370   differences in the simulated future vegetation under RCP 8.5 scenario with and without intensified ENSO are shown. The opposite behaviour of the northern parts of East Africa under El Niño vs. La Niña conditions can also be observed on NPP and RUNOFF figures, wheres for NEE differences a particular pattern is not emergent. This is mainly because NEE values can themselves be negative (flux to ecosystem) and positive (release to atmosphere).

375
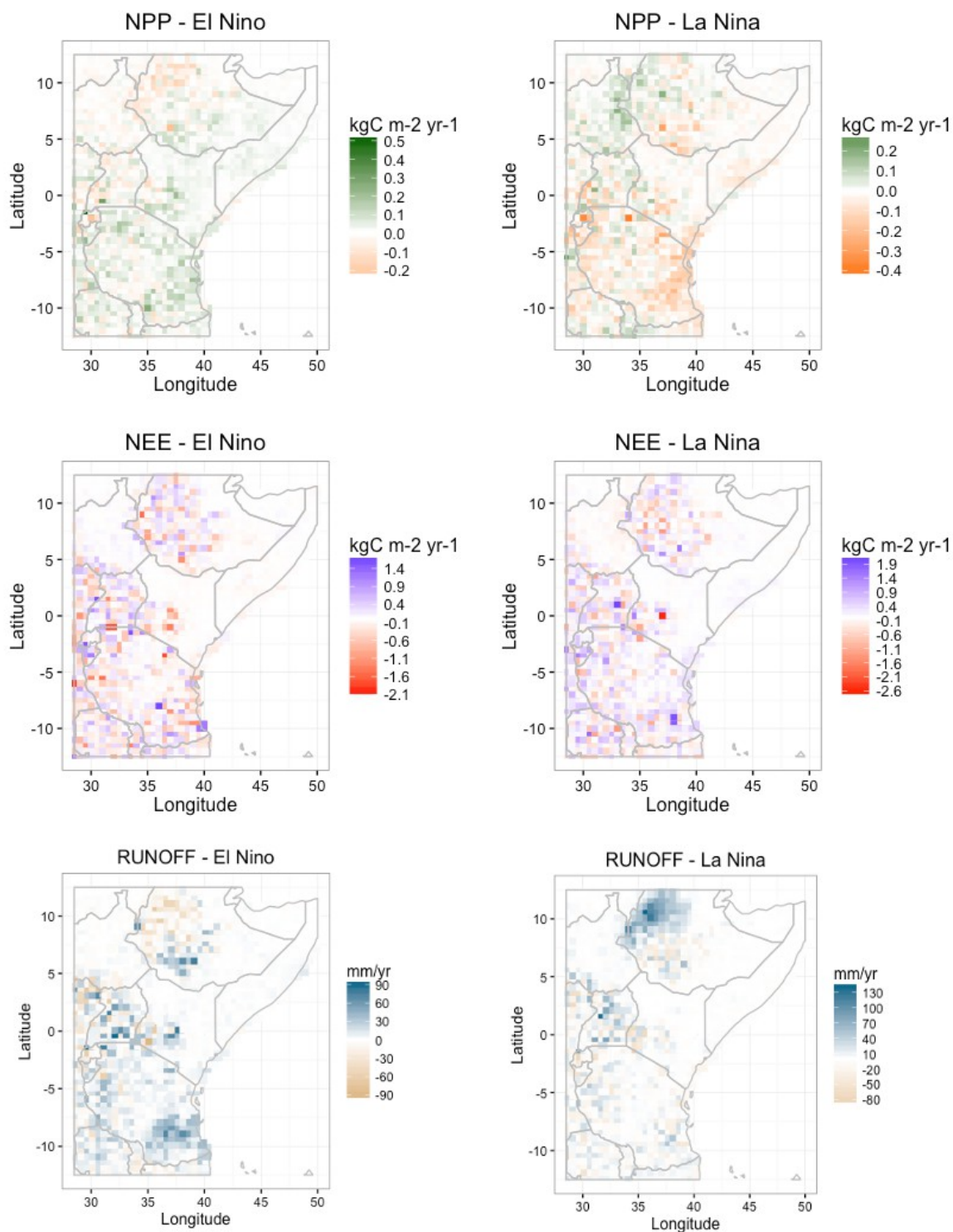
Figure 4. Simulated future differences in the NPP, NEE and RUNOFF between with and without intensified ENSO runs. (Left) Mean differences for the strong El Nino years ($\geq + 1.5°C$) (2025, 2026, 2077) were calculated by subtracting the GCM-ensemble driven simulations without modification from the GCM-ensemble driven future simulations with intensified ENSO signal. (Right) Same for strong future La Nina events ($\leq - 1.5°C$)

380 (2039, 2049, 2084, 2039, 2049, 2084).

4 Discussion

4.1 Identifying and intensifying the ENSO Signal

East African rainfall variability and especially contribution of the ENSO was investigated before (Indeje et al., 2000; Schreck and Semazzi, 2004). Here we used a different method, Empirical Orthogonal

385 Teleconnections (EOT) analysis to quantitatively calculate the ENSO contribution and found the spatial correlation patterns over the East Africa region to be in agreement with previous studies who independently looked at Pacific SST drivers for East African precipitation (Anyah and Semazzi, 2007). The ENSO signal identified through this method was also showing strong correlation with NOAA Nino3.4 index, which means EOT method was a suitable choice for our analysis.

390 Using the EOT method, we presented a conservative estimate of ENSO variability in East African rainfall, because we considered the direct Tropical Pacific teleconnection only. However, there are accompanying changes: ENSO events are linked to Indian Ocean Dipole, which more directly influences EA rainfall (Black et al., 2003). It has been suggested that subsequent to ENSO triggering, internal Indian Ocean dynamics could take over. More specifically, East African rainfall increases as

395 the western Indian Ocean gets warmer which is often associated with ENSO forcing. However, warmer western Indian Ocean can weaken the rains when it interacts with southeasterly atmospheric circulations (Schreck and Semazzi, 2004). The exact relationship and discrepancies between IOD and ENSO behaviours are yet to be revealed (Lim et al. 2016). Still, we found that the ENSO-East Africa connection to be robust as previous studies (Indeje et al., 2000; Anyah and Semazzi, 2007) and did not

400 delve into IOD relationship. Also, we were motivated by the previous studies that have identified ENSO influence to be important in dryland vegetation dynamics (Ahlström et al., 2015; Abdi et al., 2016). Hence, we focused on reporting more comparable results with those. Another factor that could affect our estimations is atmospheric latency. In our analysis, we did not consider any time lags for the tropical pacific SST anomalies and East African precipitation teleconnection, but a time lag can be

405 expected due to atmospheric circulation processes, and the influence of SST anomalies might develop instantaneously. Therefore if we account for this time lag, we might explain even more of the rainfall variance. For a more comprehensive study of SST influences on East African rainfall see Appelhans and Nauss (2016).

The EOT method, which is shown here to be effective on the historical observations, produced different

410 East African rainfall variability patterns due to Pacific SSTs when GCM outputs were used. Also the ENSO signal retrieved was much weaker than the one extracted from the observation datasets in terms of both ENSO event strength and the match (correlation) with the Nino 3.4 index. As a preliminary investigation (not shown), we conducted the EOT analysis across mixture of observed-simulated datasets: Pacific SSTs$_{observed}$ (NOAA ERSST) - East African precipitation$_{simulated}$ (CORDEX), and Pacific

415   SSTs$_{simulated}$ (GCMs) - East African precipitation$_{obsrved}$ (CRU). The ENSO signal retrieved from the

Pacific SSTs$_{observed}$ - East African precipitation$_{simulated}$ pair was a better match with Nino 3.4 index than the

one extracted from the simulated-simulated pair but still worse than the one extracted from observed-

observed dataset pair, whereas ENSO signal retrieved from the Pacific SSTs$_{simulated}$ - East African

precipitation$_{obsrved}$ pair was not a better match to Nino 3.4 index than the one extracted from the

420   simulated-simulated pair. This quick test indicated that the GCM simulated Tropical Pacific SSTs are

the main source of the poor teleconnection identified from the simulated-simulated pair and a dynamic

downscaling of the tropical Pacific SSTs might improve the ocean-atmosphere coupled teleconnection.

However, more formal tests are needed to conclude on this matter, which was beyond the scope of this

study.

425   **4.2 Present-day simulations**

Despite the fact that our estimation of ENSO contribution to the East African interannual rainfall

variability was conservative, the precipitation difference between with and without ENSO contribution

was equivalent to one or even two rainy months for some of the grid cells. These regions already

receive a small amount of rainfall and even minor differences are critical for agricultural food

430   production and the productivity of the natural ecosystem that sustains a large biodiversity. We found up

to 0.1 kgC m^{-2} yr^{-1} mean difference in NPP in the southern parts of the region solely due to ENSO

contribution.

We found that ENSO influence on net ecosystem exchange is also prominent in the semi-arid

435   ecosystems of East Africa. Especially, in southern-coastal parts, ecosystem releases more to the

atmosphere during La Nina events whereas it would store more carbon otherwise. This would also have

implications on global carbon cycle as it has previously been found that regional response of semi-arid

ecosystems, mainly occupying low latitudes, play an important role in determining the trend in CO_2

uptake by terrestrial ecosystems (Ahlström et al. 2015). For instance, La Nina events are associated with

440   large carbon sinks in Australian semi-arid ecosystems due to increased precipitation and 2011 anomaly

in global carbon sink was mainly attributed to the response of Australian ecosystems (Poulter et al.,

2014). While semi-arid ecosystems of East Africa might play a smaller role than Australian ones

(simply due to the difference in the area they cover), it would still influence the magnitude and trend of

the global carbon sink by terrestrial ecosystems. Our findings reiterate the importance of considering

445   ENSO contribution in carbon budget calculations for any region that is influenced by ENSO variability.

Here we also reported ENSO influence on surface runoff as excess runoff response causes problems in

East Africa. In this region, Rift Valley Fever (RVF) and Malaria outbreaks are threatening the livelihood

of the society and these vector-borne diseases are transmitted by mosquitoes who breed in flooded low-

lying habitats (Meegan and Bailey, 1989, Kovats et al., 2003, Hope and Thomson, 2008). For example,

450   a major RVF outbreak during late 1997 to early 1998 has been linked to the heavy and prolonged rains

that are associated with 1997-98 El Nino event (Trenberth, 1998), in agreement with our results where

we found that the southern coastal site experiences higher runoff during El Nino events than otherwise it

would do.

Another important ecological factor to be considered for East African vegetation dynamics is fire. The

455   fire occurrence in LPJ-GUESS depends on the atmospheric temperature values, and moisture and litter

availability. Therefore, although we did not calibrate LPJ-GUESS fire parameters for East Africa or

explicitly changed fire regimes under any of the scenarios, the model simulated the changes in fire

behaviour due to different environmental states implicitly. More specifically, for the southern coastal

part, a higher mean expected return time of fire was simulated during the El Nino years for simulations

460   with ENSO contribution than without due to higher moisture availability during ENSO years for this

region (not shown). For the same site, the opposite was true for La Nina years, and the whole behaviour

was reversed for the northern site. A more sophisticated fire – ENSO – vegetation interplay can be

further investigated using models that have an individual level representation of fire response such as

aDGVM2 (Scheiter, Langan and Higgins, 2013).

465   **4.3 Future simulations**

For the future simulations we intensified the ENSO signal such that very strong ENSO years can also be

experienced as it is the real-world case. Therefore, our 'intensified' version is more likely to be the

realistic version, and considering that we are expected to experience even stronger ENSO events in the

future than today (Cai et al., 2013) we could have intensified this signal even more. However, our

470   results with even this modest intensification shows the importance of capturing atmosphere-ocean

teleconnections in climate simulations for reliable future simulations of the ecosystems. We simulated

large differences in future ecosystem responses under our intensified ENSO scenario, as large as the

differences we calculated for the present-day with and without ENSO simulations. In other words, if we

were to predict vegetation response to future climate change by using GCM outputs as they are, it

475   would be as if simulating the present-day vegetation with climate data without any ENSO contribution.

Apart from the temporal and strength mismatch, the GCM simulations are also producing different

spatial patterns for tropical Pacific SST-East African rainfall teleconnection. Therefore, in our

modification we chose to correct for this spatial pattern by using the relationships we obtained from the

480   observed datasets as this correction did not influence the temporal behavior and the peakiness of the

ENSO signal retrieved from the GCM simulations. As a result, our findings can be compared for present

day patterns directly.

Especially the total surface runoff and NPP responses were considerably underestimated. Under the

intensified ENSO scenario, an excessive amount of runoff is simulated for the northern parts during La

485   Nina years and for the southern parts during El Nino years, which would exacerbate the disease events

in the region. Likewise, the simulated low amounts of runoff for the northern parts during El Nino years

indicate drought events in this parts of the region. This effect can also be seen in the simulated NPP

responses which reduces considerably for the northern parts during El Nino years. Furthermore, the

amounts we calculated here agree well with previous studies showing changes in NPP supply associated

490   with ENSO events in sub-Saharan African drylands (Abdi et al., 2016).

5 Conclusion

In this study we investigated the relationship between interannual East African rainfall variability and

495   ENSO events using Empirical Orthogonal Teleconnection (EOT) analysis, and found a robust

connection from observational datasets in agreement with previous studies. While the strength of this

relationship is not homogeneous among the region, and the patterns of vegetation response presented

opposite characteristics in the northern and southern areas, ENSO influence on East African vegetation

and in return its carbon and hydrological fluxes was apparent. However, we also found that climate

500   simulations are still not good at capturing this pertinent rainfall variability due to ENSO. This implies

that the future vegetation would be different from what is simulated under these climate model outputs

lacking accurate ENSO contribution, whereas it is important to account for this influence which can

bring further environmental stress to East Africa as we show here. Overall, our results highlight that

more robust projections on coupled atmosphere-ocean teleconnections can help reducing large

505   uncertainties of the future magnitude and sign of carbon sink provided by terrestrial ecosystems by

improving our understanding on the vegetation response.

510

Acknowledgements

IF was funded by DAAD, grants to F. J. and German Research Foundation (DFG) Graduate School GRK1364 program (Shaping Earth's Surface in a Variable Environment – Interactions between tectonics, climate and biosphere in the African-Asian monsoonal region). FJ and BT acknowledge the

515   support by the BMBF in the framework of the OPTIMASS project (01LL1302A and 01LL1302B). We thank Plant Ecology and Nature Conservation Group of Potsdam University for the inspiring discussions, and Dr. Appelhans for helpful discussions on the EOT method. We are grateful for Biogeosciences' editor comments and suggestions that helped us improve our manuscript.

520   *The authors declare that they have no conflict of interest.*

References

Abdi, A. M., Vrieling, A., Yengoh, G. T., Anyamba, A., Seaquist, J. W., Ummenhofer, C. C., Ardö, J., 2016, The El Nino - La Nina cycle and recent trends in supply and demand of net primary productivity

525   in African drylands, Climatic Change, 138:111-125, dx.doi.org/10.1007/s10584-016-1730-1

Ahlström, A., Schurgers, G., Arneth, A., Smith, B, 2012. Robustness and uncertainty in terrestrial ecosystem carbon response to CMIP5 climate change projections. Environmental Research Letters, 7(4), dx.doi.org/10.1088/1748-9326/7/4/044008

Ahlström, A., Raupach, M. R., Schurgers, G., Smith, B., Arneth, A., Jung, M.,Reichstein, M., Canadell,

530   J. G., Friedlingstein, P., Jain, A. K., Kato, E., Poulter, P., Sitch, S., Stocker, B. D., Viovy, N., Wang, Y.

P., Wiltshire, A., Zaehle, S., Zeng, N., 2015, The dominant role of semi-arid ecosystems in the trend and

variability of the land CO_2 sink, Science, 348(6237), 895-899. dx.doi.org/10.1126/science.aaa1668

Anyah, R.O., Semazzi, F.H.M., 2007, Variability of East African rainfall based on multiyear RegCM3

simulations, International Journal of Climatology, 27, 357-371. dx.doi.org/10.1002/joc.1401

535   Appelhans, T., Detsch, F., Nauss, T., 2015, remote: Empirical orthogonal teleconnections in R, Journal

of Statistical Software, 65-10. https://www.jstatsoft.org/article/view/v065i10

Appelhans, T., Nauss, T., 2016, Spatial patterns of sea surface temperature influences on East African

precipitation as revealed by empirical orthogonal teleconnections, Frontiers in Earth Science,

dx.doi.org/10.3389/feart.2016.00003

540   Bobe, R., 2006, The evolution of arid systems in eastern Africa, Journal of Arid Environments, 66(3),

564-584, dx.doi.org/10.1016/j.jaridenv.2006.01.010

Detsch, F., Otte, I., Appelhans, T., Hemp, A., Nauss, T., 2016, Seasonal and long-term vegetation

dynamics from 1-km GIMMS-based NDVI time series at Mt. Kilimanjaro, Tanzania. Remote Sensing

of Environment, 178, 70-83. http://dx.doi.org/10.1016/j.rse.2016.03.007

545 Dietrich, J. P., Schmitz, C., Lotze-Campen, H., Popp, A., Müller, C., 2014, Forecasting technological

change in agriculture – An endogenous implementation on global land use model, Technological

Forecasting & Societal Change, 81, 236-249 http://dx.doi.org/10.1016/j.techfore.2013.02.003

Endris, H. S., Omondi, P., Jain, S., Lennard, C., Hewitson, B., Chang'a, L., Awange, J.L., Dosio, A.,

Ketiem, P., Nikulin, G., Panitz, H. J., Büchner, M., Stordal, F., Tazalika, L., 2013, Assessment of the

550 performance of CORDEX regional climate models in simulating eastern Africa rainfall, Journal of

Climate. 26 (21): pp. 8453-8475, http://dx.doi.org/10.1175/JCLI-D-12-00708.1

FAO (Food and Agriculture Organization of the United Nations). 2016. FAOSTAT http://faostat.fao.org.

Fer, I., Tietjen, B., Jeltsch, F., 2015. High-resolution modelling closes the gap between data and model

simulations for Mid-Holocene and present-day biomes of East Africa. Palaeogeography,

555 Palaeoclimatology, Palaeoecology, 444, 144-151. http://dx.doi.org/10.1016/j.palaeo.2015.12.001

Gerten, D., Schaphoff, S., Haberlandt, U., Lucht, W., Sitch, S., 2004. Terrestrial vegetation and water

balance – hydrological evaluation of a dynamic global vegetation model. Journal of Hydrology, 286,

249–270. http://dx.doi.org/10.1016/j.jhydrol.2003.09.029

Goddard, L., Graham, N. G., 1999, Importance of the Indian Ocean for simulating rainfall anomalies

560 over eastern and southern Africa, Journal of Geophysical Research, 104, 19099-19116,

dx.doi.org/10.1029/1999JD900326

Harris, I., Jones, P.D., Osborn, T.J., Lister, D.H., 2014, Updated high-resolution grids of monthly climatic observations - the CRU TS3.10 dataset, International Journal of Climatology. 34, 623-642. http://dx.doi.org/10.1002/joc.3711

565   Hickler, T., Smith, B., Sykes, M.T., Davis, M. B., Sugita, S., Walker, K., 2004, Using a generalized vegetation dynamics in Northeastern USA, Ecology, 86(2), 519-530, dx.doi.org/10.1890/02-0344

Hope, L.K., Thomson, M.C., 2008, Climate and Infectious diseases. Seasonal forecasts, climatic change and human health, Springer 31-70 http://dx.doi.org/10.1007/978-1-4020-6877-5_3

Huang, B., V.F. Banzon, E. Freeman, J. Lawrimore, W. Liu, T.C. Peterson, T.M. Smith, P.W. Thorne,

570   S.D. Woodruff, H.-M. Zhang, 2014, Extended Reconstructed Sea Surface Temperature version 4 (ERSST.v4): Part I. Upgrades and intercomparisons. *Journal of Climate*, http://dx.doi.org/10.1175/JCLI-D-14-00006.1

Indeje, M., Semazzi, F. H. M., Ogallo, L. J., 2000, ENSO Signals in East African Rainfall Seasons, International Journal of Climatology, 20, 19-46(2000), dx.doi.org/10.1002/(SICI)1097-

575   0088(200001)20:1<19::AID-JOC449>3.0.CO;2-0

Ivory, S. J., Russell, J., Cohen, A. S., 2013, In the hot seat: Insolation, ENSO, and vegetation in the African tropics, Journal of Geophysical Research: Biogeosciences, 118, 1347-1358, dx.doi.org/10.1002/jgrg.20115

Kovates, R.S., Bouma, M.J., Hajat, S., Worrall, E., Haines, A., 2013, El Niño and health, Lancet,

580   362(9394), 1481-9, dx.doi.org/10.1016/S0140-6736(03)14695-8

Lim, E-P, Hendon, H. H., Zhao, M., Yin, Y., 2016, Inter-decadal variations in the linkages between

ENSO, the IOD and south-eastern Australia springtime rainfall in the past 30 years. Climate Dynamics,

1-16, dx.doi.org/10.1007/s00382-016-3328-8

Liu, W., Huang, B. , Thorne, P.W. , Banzon, V.F. , Zhang, H.-M. , Freeman, E., Lawrimore, J., Peterson,

585   T.C. , Smith, T.M., Woodruff, S.D., 2014: Extended Reconstructed Sea Surface Temperature version 4

(ERSST.v4): Part II. Parametric and structural uncertainty estimations. Journal of Climate,

dx.doi.org/10.1175/JCLI-D-14-00007.1

Meegan, J. M., C. L. Bailey, 1989, Rift Valley fever. The Arbo Viruses: Epidemiology and Ecology, T. P.

Monath, Ed., Vol. IV, CRC Press, 51–76.

590   Miralles, D. G., van den Berg, M. J., Gash, J. H., Parinussa, R. M., de Jeu, R. A. M., Beck, H. E.,

Holmes, T. R. H., Jimenez, C., Verhoest, N. E. C., Dorigo, W. A., Teuling, A. J., Dolman, A. J., 2014, El

Nino - La Nina cycle and recent trends in continental evaporation, Nature Climate Change, 4, 122-126,

dx.doi.org/10.1038/nclimate2068

Moncrieff, G.R., Scheiter, S., Bond, W.J., Higgins, S.I., 2014, Increasing atmospheric CO2 overrides the

595   historical legacy of multiple stable biome states in Africa, New Phytologist, 201(3), 908-915.

dx.doi.org/10.1111/nph.12551

Moss, R. H., Edmonds J. A., Hibbard, K. A., Manning, M. R., Rose, S.K., van Vuuren D. P., Carter, T. R., Emori, S., Kainuma, M., Kram, T., Meehl, G. A., Mithcell, J. F. B., Nakicenovic, N., Raihai, K., Smith, S. J., Stouffer, R. J., Thomson, A. M., Weyant, J. P., Willbanks, T. J., 2010, The next generation

600   of scenarios for climate change research and assessment. Nature, 463:747–756, dx.doi.org/10.1038/nature08823

Nazarenko, L., Schmidt, G.A., Miller, R.L., Tausnev, N., Kelley, M., Ruedy, R., Russell, G.L., Aleinov, I., Bauer, M., Bauer, S., Bleck, R., Canuto, M., Cheng, Y., Clune, T. L., Del Genio, A. D., Faluvegi, G., Hansen, J. E., Healy, R. J., Kiang, N. Y., Koch, D., Lacis, A. A., LeGrande, A. N., Lerner, J., Lo, K.

605   K., Menon, S., Oinas, V., Perlwitz, J. P., Puma, M. J., Rind, D., Romanou, A., Sato, M., Shindell, D. T., Sun, S., Tsigaridis, K., Unger, N., Voulgarakis, A., Yao, M.-S., Zhang, J., 2015: Future climate change under RCP emission scenarios with GISS ModelE2. J. Adv. Model. Earth Syst., **7(**1), 244-267, dx.doi.org/10.1002/2014MS000403

Nicholson, S.E., 2000. The nature of rainfall variability over Africa on time scales of decades to

610   millenia. Global and Planetary Change 26, 137–158. http://dx.doi.org/10.1016/S0921-8181(00)00040-0

Nicholson, S.E., 2014, A detailed look at the recent drought situation in the Greater Horn of Africa, *Journal of Arid Environments*, 103, 71-79. dx.doi.org/10.1016/j.jaridenv.2013.12.003

Nicholson, S. E., 2015, Long-term variability of the East African 'short-rains' and its links to large-scale factors, International Journal of Climatology, 35(13), 3979-3990, http://dx.doi.org/10.1002/joc.4259

615 Nikulin, G., Jones, C., Giorgi, F., Asrar, G., Büchner, M., Cerezo-Mota, R., Christensen, O., Deque, M., Fernandez, J., Hänsler, A., van Meijgaard, E., Samuelsson, P. Sylla, M. B., Sushama, L., 2012, Precipitation climatology in an ensemble of CORDEX-Africa regional climate simulations, American Meteorological Society, 25, 6058-6078, dx.doi.org/10.1175/JCLI-D-11-00375.1

Poulter, B., Frank, D., Ciais, P., Myneni, R. B., Andela, N., Bi, J., Broquet, G., Canadell, J. G.,
620 Chevallier, F., Liu, Y. Y., Running, S. W., Sitch, S., van der Werf, G., 2014, Contribution of semi-arid ecosystems to interannual variability of global carbon cycle, Nature, 509, 600-603, dx.doi.org/10.1038/nature13376

R Core Team (2015). R: A Language and Environment for Statistical Computing. R Foundation for Statistical Computing, Vienna, Austria. URL http://www.R-project.org/

625 Riahi, K., Rao, S., Krey, V., Cho, C., Chirkov, V., Fischer, G., Kindermann, G., Nakicenovic, N., Rafaj, P., 2011, RCP 8.5 – A scenario of comparatively high greenhouse gas emissions. Climatic Change, 109:22, dx.doi.org/10.1007/s10584-011-0149-y

Ropelewski, C.F., Halpert, M.S., 1996, Quantifying Southern Oscillation-rainfall relationships, *Journal of Climate*, 9, 1043-1059. dx.doi.org/10.1175/1520-0442(1996)009<1043:QSOPR>2.0.CO;2

Sanford. T., Frumhoff, P. C., Luers, A., Gulledge, J., 2014, The climate policy narrative for a dangeroously warming world. Nature Climate Change, 4, 164-166, dx.doi.org/10.1038/nclimate2148

Scheiter, S., Langan, L., Higgins, S. I., Next-generation dynamic global vegetation models: learning from community ecology. New Phytologist, 198(3), 957-969. dx.doi.org/10.1111/nph.12210

635 Scheiter, S., Savadogo, S., 2016, Ecosystem management can mitigate vegetation shifts induced by climate change in West Africa, Ecological Modelling, 332, 19-27, http://dx.doi.org/10.1016/j.ecolmodel.2016.03.022

Schreck, C. J, Semazzi, F. H. M., 2004, Variability of the recent climate of East Africa, International Journal of Climatology, 24:681-701, dx.doi.org/10.1002/joc.1019

640 Shisanya, C. A., Recha, C., Anyamba, A., 2011, Rainfall variability and its impact on Normalized Difference Vegetation Index in arid and semi-arid lands of Kenya, International Journal of Geosciences, 2, 36-47, dx.doi.org/10.4236/ijg.2011.21004

Sitch, S., Smith, B., Prentice, I.C., Arneth, A., Bondeau, A., Cramer, W., Kaplan, J.O., Levis, S., Lucht, W., Sykes, M.T., Thonicke, K., Venevsky, S., 2003. Evaluation of ecosystem dynamics, plant geography
645 and terrestrial carbon cycling in the LPJ dynamic global vegetation model. Global Change Biology. 9, 161−185. http://dx.doi.org/10.1046/j.1365-2486.2003.00569.x

Smith, B., Prentice, I.C., Sykes, M.T., 2001. Representation of vegetation dynamics in the modelling of terrestrial ecosystems: comparing two contrasting approaches within European climate space. Global Ecology and Biogeography. 10, 621−637. http://dx.doi.org/10.1046/j.1466-822X.2001.t01-1-00256.x

650   Thonicke, K., Venevsky, S., Sitch, S., Cramer, W., 2001, The role of fire disturbance for global

vegetation dynamics: coupling fire into a dynamic vegetation model, Global Ecology and

Biogeography, 10(6), 661-67, dx.doi.org/10.1046/j.1466-822X.2001.00175.x

Thornton, P.K., Ericksen, P.J., Herrero, M., Challinor, A.J., 2014, Climate variability and vulnerability

to climate change: a review, *Global Change Biology*, 20, 33-13-3328. dx.doi.org/10.1111/gcb.12581

655   Trenberth, K. E., 1998, Forecasts of the development of the 1997- 98 El Niño event. *CLIVAR*

Exchanges, Vol. 3, No. 2/3, 4–14. http://www.cgd.ucar.edu/cas/papers/clivar98_Santiago

van den Dool, H.M., Saha, S., Johansson, A., 2000, Empirical orthogonal teleconnections, *Journal of*

Climate, 13 (8), 1421-1435. dx.doi.org/10.1175/1520-0442(2000)013<1421:EOT>2.0.CO;2

Vecchi, G. A., Wittenberg, A. T., 2010, El Nino and our future climate: where do we stand?, WIREs

660   Climate Change, 1(1), 260-270, dx.doi.org/10.1002/wcc.33

Waha, K., Müller, C., Bondeau, A., Dietrich, J.P., Kurukulasuriya, P., Heinke, J., Lotze-Campen, H.,

2013, Adaptation to climate change through he choice of cropping system and sowing date in sub-

Saharan Africa, Global Environmental Change, 23, 130-143.

http://dx.doi.org/10.1016/j.gloenvcha.2012.11.001

665   Wolff, C., Haug, G.H., Timmermann, A., Damste, J.S.S, Brauer, A., Sigman, D.M., Cane, M.A.,

Verschuren, D., 2011, Reduced interannual rainfall variability in East Africa during the Last Ice Age,

Science, 333, 743. dx.doi.org/10.1126/science.1203724

Appendix A

A1 Code

670 All the R code used in this study can be found at github.com/istfer/ENSOpaper

675

680

A2 Figures
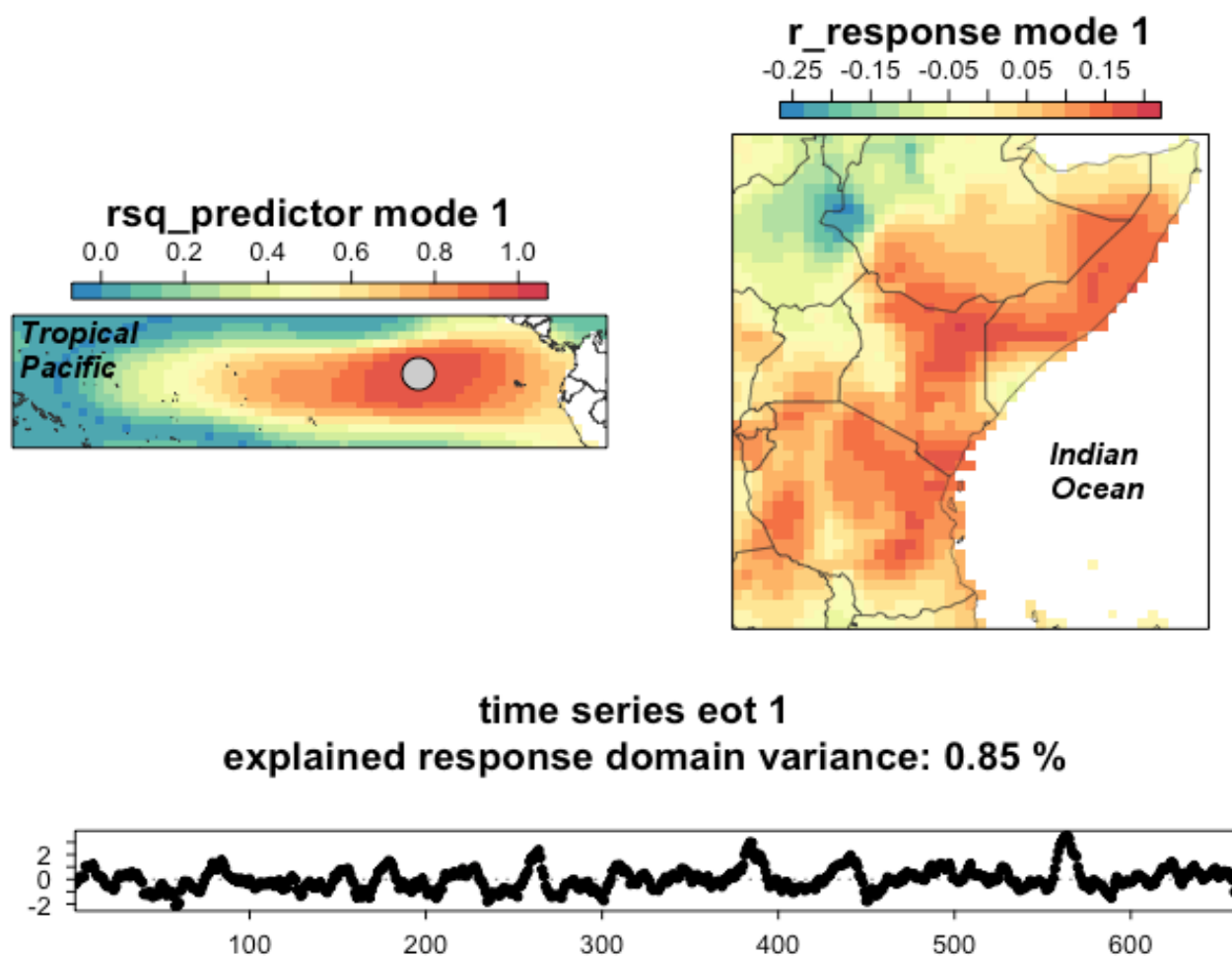
685   Figure A1. Coupled ocean-atmosphere teleconnection between Pacific Sea Surface Temperatures and East

African Rainfall retrieved from historical observations. (Upper Left) The coefficients of determination for the

predictor field highlights that the Nino-3.4 region explains the variance in the response domain the most. (Upper

Right) Correlation coefficients of the each pixel of the East Africa (response) domain shows that spatially the

coastal parts and a north-western area is being explained by the predictor field. (Bottom panel) Time series of

690   Tropical Pacific SST anomalies at the base point (the gray circle in the upper left panel) of the first mode as

ENSO signal.
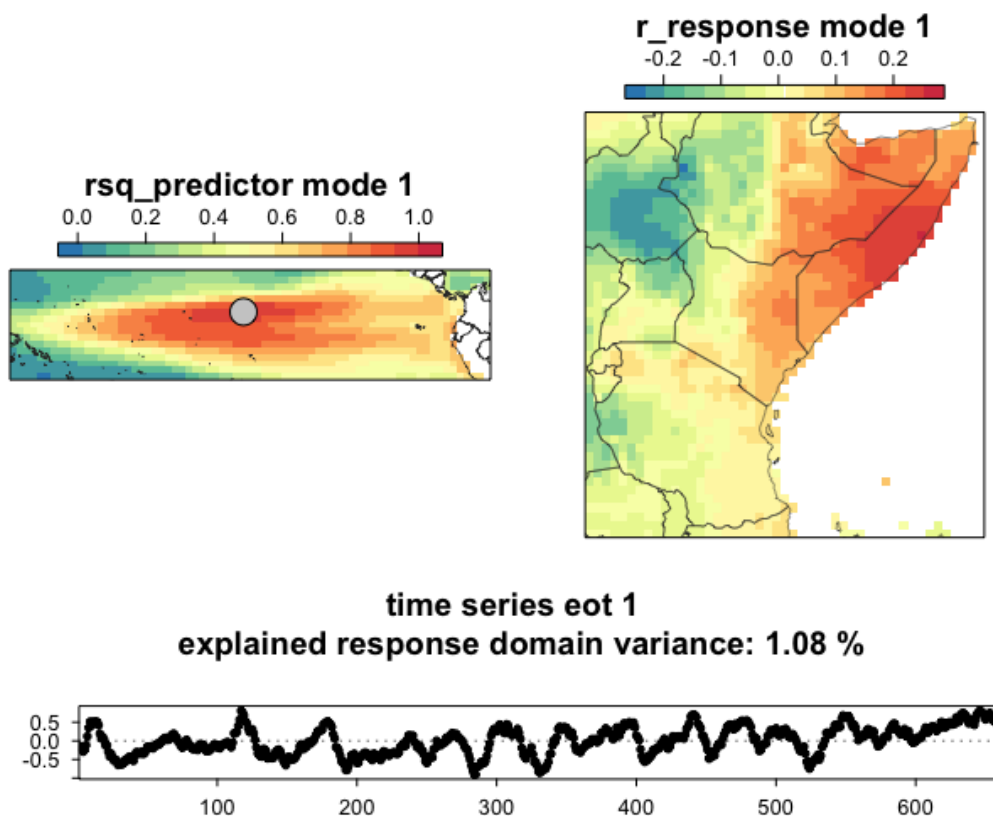
Figure A2. EOT Analysis for the historical period from the GCM simulations. Panels as explained in Figure A1:

695   (Left) The coefficients of determination for the predictor field. (Right) Correlation coefficients of the each pixel

of the East Africa (response) domain. (Bottom) Time series at the base point of the mode.
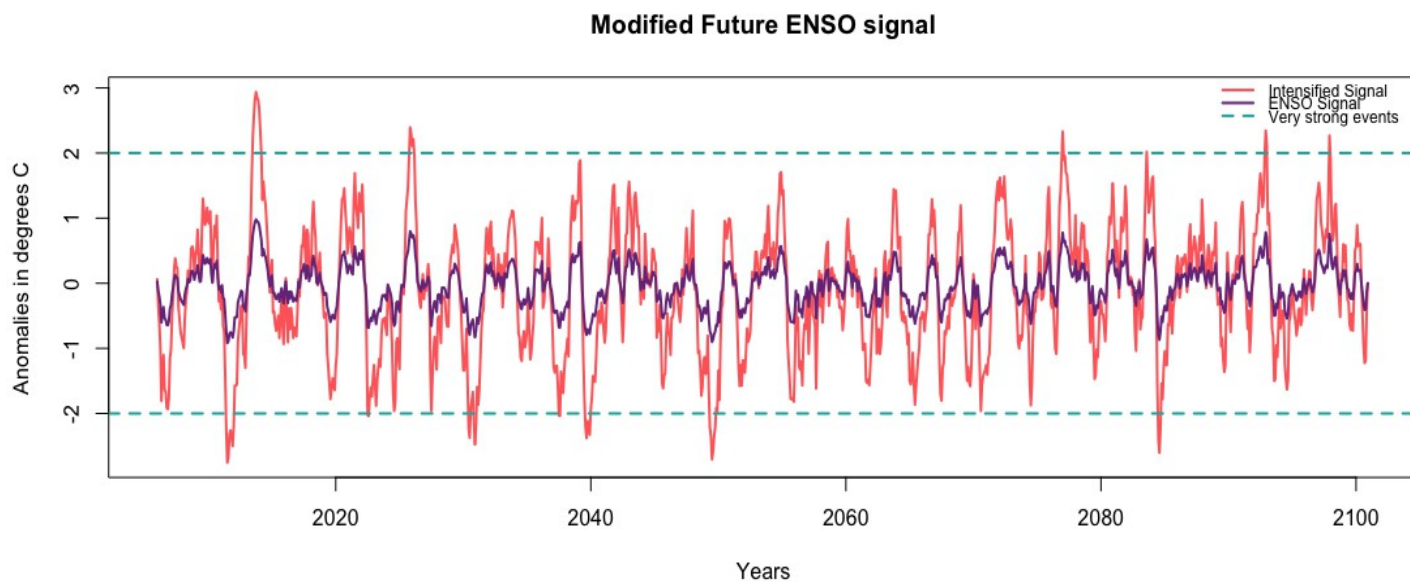
700   Figure A3. Intensified ENSO signal. Purple line: Future ENSO signal retrieved from GCM outputs for 2006-2100

period. Red Line: Intensified signal such that anomalies peak as strong as recorded amplitudes (± 2.5° C)

.Dashed line marks the very strong ENSO event threshold..

705

A3 Full names of Global Circulation Models and their home Institutions

CCCma-CanESM2: Canadian Centre for Climate Modelling and Analysis - The second generation Canadian

710   Earth System Model (Flato et al., 2000)

CERFACS CNRM-CM5: Centre Européen de Recherche et de Formation Avancée, Centre National de Recherches

Météorologiques, Climate Model 5 (Voldoire et al., 2013)

IPSL CM5A-MR: Institut Pierre Simon Laplace Climate Model 5A Medium Resolution (Hourdin et al., 2013)

QCCCE CSIRO Mk3-6-0: Queensland Climate Change Centre of Excellence, Commonwealth Scientific and

715   Industrial Research Organization, Mark 3.6 (Collier et al., 2013)

ICHEC EC-EARTH: Irish Centre for High End Computing, EC-Earth (Sterl et al., 2012)

MIROC5: Atmosphere and Ocean Research Institute (The University of Tokyo), National Institute for

Environmental Studies, and Japan Agency for Marine-Earth Science and Technology, Model for Interdisciplinary

Research on Climate (Watanabe et al., 2010)

720   MPI-M ESM-LR: Max Planck Institute for Meteorology, Earth System Model, Low Resolution (Giorgetta et al.,,

2013)

NCC NorESM1-M: Norwegian Climate Centre, Norwegian Earth System Model (Bentsen et al., 2013)

NOAA GFDL-ESM2M: National Oceanic and Atmospheric Administration, Geophysical Fluid Dynamics

Laboratory (Dunne et al., 2012)

725

References

Bentsen, M., et al. (2013): The Norwegian Earth System Model, NorESM1-M - Part 1: Description and basic evaluation of the physical climate, Geosci. Model Dev., 6, 687-720, doi:10.5194/gmd-6-687-2013

Collier, M. et al., 2013, Ocean circulation response to anthropogenic-aerosol and greenhourse gas forcing in the CSIRO-Mk3.6 coupled climate model, Australian Meteorological and Oceanographic Journal, 63, 27-39

Dunne, J.P, et al., 2012, GFDL's ESM2 Global Coupled Climate-Carbon Earth System Models, American Meteorological Society, http://dx.doi.org/10.1175/JCLI-D-11-00560.1

Flato, G. M. et al., 2000. "The Canadian Centre for Climate Modeling and Analysis global coupled model and its climate". Climate Dynamics. **16** (6): 451–467. doi:10.1007/s003820050339.

Giorgetta, M., et al. 2013, Climate change from 1850 to 2100 in MPI-ESM simulations for the coupled model intercomparison project phase 5, J. Adv. Model. Earth Syst., doi:10.1002/jame.20038

Hourdin, F., Foujols, MA., Codron, F. et al., 2013, Clim Dyn, 40: 2167. doi:10.1007/s00382-012-1411-3

Sterl, A., Bintanja, R., Brodeau, L. et al., 2012, Clim Dyn, 39: 2631. doi:10.1007/s00382-011-1239-2

Voldoire, A., Sanchez-Gomez, E., Salas y Mélia, D. et al. Clim Dyn (2013) 40: 2091. doi:10.1007/s00382-011-1259-y

Watanabe, M., et al., 2010, Improved Climate Simulation by MIROC5: Mean States, Variability, and Climate Sensitivity, American Meteorological Society, http://dx.doi.org/10.1175/2010JCLI3679.1